

UCLA

UCLA Previously Published Works

Title

High-Sensitivity Intrinsic Optical Signal Imaging Through Flexible, Low-Cost Adaptations of an Upright Microscope

Permalink

<https://escholarship.org/uc/item/4bf478t4>

Journal

eNeuro, 10(8)

ISSN

2373-2822

Authors

Vasquez, Brenda
Campos, Baruc
Cao, Ashley
[et al.](#)

Publication Date

2023-07-01

DOI

10.1523/eneuro.0046-23.2023

Copyright Information

This work is made available under the terms of a Creative Commons Attribution License, available at <https://creativecommons.org/licenses/by/4.0/>

Peer reviewed

1. Manuscript Title: High sensitivity intrinsic optical signal imaging through flexible, low-cost adaptations of an upright microscope

2. Abbreviated Title: Open source tools to enable intrinsic signal imaging

3. Author Names & Affiliations: Brenda Vasquez¹, Baruc Campos¹, Ashley Cao, Aye Theint Theint, and William Zeiger*

Department of Neurology, David Geffen School of Medicine, University of California Los Angeles, Los Angeles, CA 90095, USA

¹These authors contributed equally to this work.

4. Author Contributions: BV designed and performed research, analyzed data, and wrote the paper; BC designed and performed research and analyzed data; AC performed research; ATT performed research; WZ designed and performed research, analyzed data, and wrote the paper.

5. Correspondence should be addressed to:

William Zeiger, M.D., Ph.D.
Department of Neurology, UCLA
710 Westwood Plaza, A-125
Los Angeles, CA 90025
wzeiger@mednet.ucla.edu

6. Number of Figures: 6

7. Number of Tables: 0

8. Number of Multimedia: 0

9. Number of words for Abstract: 230

10. Number of words for Significance Statement: 55

11. Number of words for Introduction: 472

12. Number of words for Discussion: 1121

13. Acknowledgements: We thank Thorlabs for loaning the CMOS camera used in this study and Dr. Carlos Portera-Cailliau for advice and helpful feedback.

14. Conflict of Interest: Authors report no conflict of interest

15. Funding Sources: This work was supported by National Institutes of Health Grant 1K08NS114165-01A1 and American Academy of Neurology Grant NRTS 2199.

High sensitivity intrinsic optical signal imaging through flexible, low-cost adaptations of an upright microscope

Abstract

Intrinsic optical signal imaging (IOSI) is a staple technique in modern neuroscience. Pioneered over thirty years ago, IOSI allows macroscopic mapping of neuronal activity throughout the cortex. The technique has been used to study sensory processing and experience-dependent plasticity, and is often used as an adjunctive procedure to localize cortical areas for subsequent targeting by other imaging or physiology techniques. Despite the ubiquity of IOSI in neuroscience there are few commercially available turn-key IOSI systems. As a result, investigators have typically resorted to building their own imaging systems. Over the years, simplified systems built either as dedicated rigs or incorporated into existing microscope platforms have been developed. Here we present a straightforward set of adaptations that can be applied to any standard upright microscope, using readily available, inexpensive, commercial parts for illumination, optics, and signal detection, that enables high sensitivity IOSI. Using these adaptations, we are able to readily map sensory-evoked signals across the somatosensory and visual cortex, including single-whisker barrel cortical activity maps in mice. We show that these IOSI maps are highly reproducible across animals and can be used to study plasticity mechanisms in the somatosensory cortex. We also provide open-source applications to control illumination and analyze raw data to generate activity maps. We anticipate these resources will be useful for neuroscience investigators looking to add IOSI capabilities to an existing microscope in the lab on a budget.

Significance Statement

Intrinsic signal optical imaging allows macroscopic detection of cortical activity. It has become a staple technique for modern neuroscience, yet there are few commercially available systems. Here we describe low-cost adaptations and open-source tools that enable the adaptation of an existing upright microscope to perform high sensitivity intrinsic signal imaging experiments and basic data analysis.

Introduction

Intrinsic optical signal imaging (IOSI) is a macroscopic imaging technique that can indirectly map neuronal activity by measuring changes in intrinsic signals (Frostig and Chen-Bee, 2009). Pioneered in the 1980s (Grinvald et al., 1986), IOSI has since become a staple technique in neuroscience. IOSI has been used to uncover the functional architecture of the brain, including the retinotopic (Crair et al., 1997; Schuett et al., 2002), somatotopic (Masino et al., 1993; Narayan et al., 1994), tonotopic (Bakin et al., 1996; Kalatsky et al., 2005), and odorant (Rubin and Katz, 1999) mapping of the cortex. It has also been critical for studies of cortical plasticity (Drew and Feldman, 2009; Dubroff et al., 2005; Kalogeraki et al., 2017; Lehmann and Löwel, 2008; Polley et al., 2004, 1999; Prakash et al., 1996; Smith and Trachtenberg, 2010; Trachtenberg et al., 2000) and to study the pathogenesis of diseases such as migraines (Ba et al., 2002), seizures (Chen et al., 2000), stroke (Clarkson et al., 2013; Harrison et al., 2013; Johnston et al., 2013), and neurodevelopmental disorders (Arnett et al., 2014; He et al., 2019). From a practical standpoint, IOSI can be used to localize cortical areas for subsequent interventions like viral vector injections (Augustinaite and Kuhn, 2021), two-

photon imaging (de Vries et al., 2020; He et al., 2017), in vivo electrophysiology (Nsiangani et al., 2022), or focal lesions (Zeiger et al., 2021).

To conduct IOSI, one needs a light source to illuminate the cortex, optics to collect reflected light, and a detector (Frostig and Chen-Bee, 2009; Zepeda et al., 2004). Many different approaches to assembling these basic hardware components have been described, with most custom-built by individual labs as there are few complete commercial IOSI set-ups available. Early set-ups for IOSI evolved from traditional upright microscopes with arrays of photodetectors (Grinvald, 1985; Grinvald et al., 1986) to a tandem lens macroscope configuration with sensitive CCD cameras (Ratzlaff and Grinvald, 1991). Illumination has shifted from broadband light sources with emission filters (Frostig et al., 1995; Ratzlaff and Grinvald, 1991) to simpler wavelength-specific light-emitting diodes (LEDs) (Augustinaite and Kuhn, 2021; Harrison et al., 2009; Salzberg et al., 2005). Here, we incorporate aspects of prior IOSI designs and provide updated protocols that enable the addition of IOSI capabilities to an existing upright microscope. We use an inexpensive, commercially available LED ring light controlled by an Arduino microcontroller for illumination, a basic microscope objective for light collection, and mid-range cameras for detection to achieve high-sensitivity IOSI. In addition, we provide simple, easy-to-use MATLAB based applications for illumination control and basic image analysis. This IOSI set up enables one to incorporate this versatile technique into the laboratory in a matter of hours for a very low budget. We anticipate it will be particularly useful for researchers performing IOSI in conjunction with other techniques requiring microscopy, such as two-photon in vivo imaging.

Methods

Experimental Animals: All experiments followed the U.S. National Institutes of Health guidelines for animal research, under an animal use protocol approved by the University of California Los Angeles Animal Research Committee (ARC). Male and female mice were used, beginning at 7-10 weeks old at the time of cranial window surgery. All animals were housed in a vivarium with a 12 h light/dark cycle. For these experiments we used 1 wild-type C57BL/J6 mouse, 3 hemizygous transgenic Ai162D mice (Ai162(TIT2L-GC6s-ICL-tTA2)-D, Jax line 031562) (Daigle et al., 2018), 3 homozygous and 7 heterozygous PV-Cre mice (B6.129P2-Pvalbtm1(cre)Arbr/J, Jax line 017320) (Hippenmeyer et al., 2005), 2 PV-Cre: Ai162 double transgenic mice, and 1 Thy1-jRGECO1a transgenic mouse (Jax line 030526) (Dana et al., 2018). All transgenic lines were maintained on a C57BL/J6 background.

Cranial Window Surgery: Implantation of chronic glass cranial windows was performed according to previously published protocols (Holtmaat et al., 2009; Mostany and Portera-Cailliau, 2008). Mice were deeply anesthetized using 5% isoflurane followed by maintenance with 1.5-2% isoflurane. The scalp was removed and periosteum cleaned away by gentle scraping. An ~4 mm diameter circular craniotomy, centered ~3 mm lateral to the midline and ~2 mm caudal to Bregma was made using a pneumatic dental drill with a FG ¼ drill bit (Midwest Dental) over the primary somatosensory cortex, including the barrel field (S1BF), forelimb (S1FL) and hindlimb (S1HL) areas. For primary visual cortex (V1), the craniotomy location was shifted ~1.5 mm caudal. The craniotomy was sealed

using either a single 5 mm #1 sterile glass coverslip (Harvard Apparatus), or a 4 mm coverslip glued to a 5 mm coverslip using an optical adhesive (Norland Products, #71), and was glued to the skull with cyanoacrylate glue (Krazy Glue) followed by dental acrylic (OrthoJet, Lang Dental). A small stainless steel headbar was placed rostral to the cranial window and embedded in dental acrylic to allow subsequent fixation of the mouse onto the microscope stage. Carprofen (5 mg/kg, i.p., Zoetis) and dexamethasone (0.2 mg/kg, i.p., Vet One) were provided for pain relief and mitigation of edema on the day of surgery and daily for the next 48 h. Mice were allowed to recover from the surgery for 3 weeks before the first imaging session. For thinned skull imaging, an ~3 mm diameter circle over S1BF was thinned until transparency using a pneumatic dental drill with a FG ¼ drill bit (Midwest Dental), followed by headbar implantation and acute IOSI.

IOSI Hardware/Software Setup: We adapted an upright two-photon microscope (Bergamo II, Thorlabs) to perform intrinsic signal imaging. A 4x air immersion objective (Nikon CFI Plan Apochromat Lambda, 0.2 NA) was threaded into the microscope objective holder and a ring of 16 LEDs with integrated drivers (Adafruit NeoPixel Ring, #1463) was affixed to the objective using a custom 3D-printed holder. The ring LED illumination was controlled using an Arduino microcontroller (Uno Rev3) and a custom written MATLAB (Mathworks) application. Full details on how to install and set-up the ring LED illumination, including files for 3D printing and MATLAB code can be found on github <https://github.com/zeigerlab/Intrinsic-Signal-Imaging>. Light from the objective was transmitted directly to a camera tube and camera, either a 1x camera tube (Thorlabs WFA4100) coupled to an 8 megapixel CCD camera (Thorlabs, 8051M-USB; 3296 x 2472

pixels, 5.5 μm x 5.5 μm pixel size, 14 bit depth, 20,000 e^- charge capacity) or a 0.5x camera tube (Thorlabs WFA4102) coupled to a 12.3 megapixel CMOS camera (Thorlabs, CS126MU; 4096 x 3000 pixels, 3.45 μm x 3.45 μm pixel size, 12 bit depth, $\geq 10,650 e^-$ charge capacity). A 5 V TTL pulse generated 1 second prior to the onset of stimuli was used to trigger camera acquisition (Thorlabs, TSI-IOBOB).

IOSI Acquisition: Animals were sedated with chlorprothixene (~ 3 mg/kg, i.p.), lightly anesthetized with ~ 0.5 - 0.7% isoflurane, and head-fixed below the microscope. The cortical surface was illuminated by green light (525 nm) to visualize and capture an image of the superficial vasculature. The microscope was then focused 300 μm below the cortical surface and red light (625 nm) was used to record intrinsic signals, with frames collected at 10 Hz starting 1 s before and up to 3 s after stimulation onset. For one mouse, we also performed IOSI using a frame acquisition rate of 30 Hz. Thirty trials with inter-stimulus intervals of 20 s were conducted for each imaging session. Paw and whisker stimuli (10 or 100 Hz sine wave, 1.5 seconds long) were generated in MATLAB, output via a multifunction input/output device (National Instruments, BNC 2090a and PCIe-6363) to a voltage amplifier (Micromechatronics, PD200-V100,100), and delivered using a glass capillary affixed to a piezoelectric bending actuator (Bimitech Python PBA6014-5H200). Visual stimuli were generated using PsychoPy (Peirce et al., 2019) and consisted of drifting sinusoidal gratings (spatial frequency 0.04 cycles/deg; speed 2 cycles/s) at orientations of 0, 45, 90, and 135° (each displayed for 0.375 seconds for a total stimulus duration of 1.5 seconds) followed by a black screen during the inter-stimulus interval.

Images were acquired with 100 ms exposure time at 10 frames per second, for a total of 4 seconds per trial.

Quantification of Evoked Signals: Images were first gaussian filtered using the `imgaussfilt` function in MATLAB, with the default kernel size of $2*\text{ceil}(2*\text{sigma})+1$, with $\text{sigma}=0.5$. Images were then spatially downsampled by a factor of four. For each trial, an average baseline reflectance image was created by calculating the mean across 0.9 s of images (9 frames) prior to stimulus onset. Post-stimulus reflectance images were temporally averaged across 0.3 s bins for 1.5 seconds total, starting 0.5 s after stimulus onset, yielding 5 post-stimulus images per trial. Change in reflectance values ($\Delta R/R$) were then calculated by subtracting the average baseline reflectance from each post-stimulus image and dividing the result by the average baseline reflectance. These $\Delta R/R$ values were then averaged across all 30 trials and finally summed across the 5 post-stimulus images to yield a single total stimulus-evoked $\Delta R/R$ image. A circular mask corresponding to the area of the cranial window (based on the vasculature image) was fit to the stimulus evoked $\Delta R/R$ image such that pixels outside the cranial window were set to 0. Binary images were then created either by thresholding $\Delta R/R$ values using a percentage of the maximum signal intensity (for larger maps, such as S1BF or V1), or by first calculating Z-scores of the obtained $\Delta R/R$ values and then thresholding values below a Z-score of -3 (for smaller maps, such as single whisker, S1FL, or S1HL). Binarized images were then pseudocolored and overlaid onto images of the vasculature. To obtain group averaged images and map displacements, binarized maps of the S1BF, S1FL, and S1HL were fit with an ellipse using the “Analyze Particles” function in Fiji/ImageJ (Schindelin et al.,

2012). The center of each ellipse was determined and stimulus evoked $\Delta R/R$ images from each mouse were aligned using the center of the S1BF ellipse, overlaid, and averaged. Displacement of S1FL and S1HL relative to S1BF were then calculated for each mouse and compared using a one-way multivariate analysis of variance (MANOVA). To quantify map area for single whisker evoked maps, the medfilt2 function in MATLAB was used to apply a median filter with a 3x3 pixel neighborhood size to binarized maps to remove noise and the area of thresholded pixels was calculated. Pre- and post-whisker trimming map sizes were compared using a paired sample, two-tailed t-test. All values listed or plotted are mean \pm standard error of the mean, unless otherwise specified.

Whisker Trimming: Animals were anesthetized with isoflurane (5% for induction, 1.5-2% for maintenance) and all whiskers on the right side of the snout, except those undergoing stimulation (B1, C1, and/or D1), were trimmed using a fine scissors to a length of ~5 mm immediately prior to imaging. For the chronic whisker trimming experiment, all whiskers on the right side of the face except C1 were trimmed flush with the vibrissal pad immediately following baseline imaging and re-trimmed as needed to remove any whisker re-growth, approximately three times weekly, for a total of three weeks.

Code Accessibility: The code/software described in the paper is freely available online at <https://github.com/zeigerlab/Intrinsic-Signal-Imaging>. The code is available as Extended Data.

Results

To adapt an existing upright microscope for IOSI, we designed a simple, easy to implement system for sample illumination and image acquisition (**Fig. 1A**). The brain surface is illuminated using an array of LEDs and reflected light is collected through a 4x microscope objective and transmitted to a scientific camera without any intervening filters (**Fig. 1B**). For sample illumination, we used a pre-fabricated LED ring light controlled by an Arduino microcontroller (see Methods). These LEDs have integrated drivers and require only a basic 5 V AC/DC power adapter. The ring light is slipped onto a 4x microscope objective using a 3D printed mount and provides even sample illumination at wavelengths of ~470 nm, ~525 nm, or ~625 nm. Control of the illumination wavelength and light intensity is achieved with a MATLAB-based application (**Fig. 1C**). Camera acquisition can then be synchronized to stimuli of interest via a transistor-transistor logic (TTL) pulse from the imaging computer. After image acquisition, images are processed using a MATLAB-based application (**Fig. 1D**) to generate scaled change in reflectance ($\Delta R/R$) images, or further thresholded and overlaid onto an image of the brain vasculature for localization of signals. The image analysis application is flexible with customizable inputs for specific acquisition settings, including imaging framerate, number of trials, baseline and stimulus duration, and temporal binning, among others (**Fig. 1D**). The entire system can be set up on an upright microscope in a few hours for a cost of <\$5000, or <\$50 if the microscope already has an appropriate objective and camera. Complete installation instructions and design files are freely available online (<https://github.com/zeigerlab/Intrinsic-Signal-Imaging>).

IOSI is commonly used to localize areas of the mouse S1. Using our set-up, we performed IOSI through a chronic cranial window implanted over the left primary somatosensory cortex during vibrotactile stimulation of the contralateral whiskers, forelimb, or hindlimb (**Fig. 2A**). We were able to record robustly evoked signals corresponding to the barrel field (S1BF), forelimb (S1FL), or hindlimb (S1HL) in individual mice (**Fig. 2B**). We then aligned the S1BF signals across 6 different animals and found that the group averaged signal for each sensory area was highly localized (**Fig. 2C**), demonstrating that the location of these maps is consistent and reproducible across animals. By thresholding and merging the S1BF, S1FL, and S1HL signals, we could clearly define distinct maps situated as expected anatomically (**Fig. 2A,D**) (Lau et al., 2008). We next quantified the relative displacement of the center of the S1FL and S1HL maps relative to the center of the S1BF map in each of six mice (**Fig. 2E**). The displacements were tightly clustered by map (S1FL or S1HL) with the S1FL map displacements significantly distinct from the S1HL map displacements (MANOVA, $p=1.04 \times 10^{-5}$). We also performed IOSI during presentation of drifting sinusoidal gratings to map the primary visual cortex and found robust visually evoked signals (**Fig. 2F,G**). Together, these results demonstrate that our IOSI set-up is sufficiently sensitive to record evoked signals from several major cortical sensory areas.

We next tried to record evoked signals from smaller cortical areas. The mouse S1BF exhibits strong somatotopic organization, with sensory signals from individual whiskers predominantly encoded within single cortical columns, or barrels, that are ~200-300 μm in diameter (Petersen, 2019). We performed IOSI during vibrotactile stimulation

of single whiskers (either the B1, C1, or D1 whisker) and recorded robust single-whisker evoked signals (**Fig. 3A,B**). After thresholding and binarizing to obtain single-whisker maps, we merged the three individual single-whisker maps and found these were clearly distinct and adjacently arranged according to the expected somatotopic organization of the S1BF (**Fig. 3C**). To quantify the minimum number of trials necessary to obtain reliable single-whisker maps, we calculated the cumulative change in reflectance values ($\Delta R/R$) across each of the 30 trials performed in an individual IOSI session for 18 single-whisker maps (3 whiskers in each of 6 mice). We then calculated the area of the evoked signal for each trial as a percentage of the maximum area obtained using all 30 trials (**Fig. 3D**). We found that map area plateaued after 25-30 trials, but was already greater than 50% of the total map area after as few as 10 trials. Faster frame acquisition rates can improve signal-to-noise ratios for IOSI, especially with lower sensitivity cameras. We found imaging at 10 Hz yielded a qualitatively similar single-whisker map compared to imaging at 30 Hz (**Fig. 3-1A**). Single-whisker maps could also be readily obtained acutely through thinned-skull preparations (**Fig. 3-1B**). Finally, we confirmed that we could generate qualitatively similar single-whisker maps to those obtained with a CCD camera using a more cost-efficient CMOS camera (**Fig. 4A-B**) and that there was no significant difference in average map size and mean map pixel intensity comparing IOSI performed with the CCD or CMOS camera (**Fig. 4C-D**). It is likely that the CCD camera could achieve higher signal-to-noise ratios compared to the CMOS camera by binning pixels on the CCD sensor, but we did not test that directly here. However, we can conclude that our IOSI set-up can incorporate both CCD and CMOS cameras to produce reliable sensory-evoked maps even from signals generated by relatively small cortical areas.

In addition to localizing signals, IOSI can be used to study cortical map plasticity. One of the most commonly used paradigms for inducing cortical map plasticity in rodents is whisker trimming. Following chronic trimming of whiskers, cortical map areas corresponding to the spared whisker expand, whereas those corresponding to trimmed whiskers shrink (Drew and Feldman, 2009; Gao et al., 2017; Polley et al., 1999). Therefore, we tested whether we could measure plasticity of single whisker maps in response to whisker trimming. Following baseline IOSI imaging of C1 whisker evoked maps (**Fig. 5A,B** left panels), we chronically trimmed all whiskers of the contralateral vibrissal pad except C1. Three weeks later we repeated IOSI during C1 whisker stimulation and quantified the area of the evoked C1 map (**Fig. 5A,B** right panels). We merged the resulting pre- and post-whisker trimming maps and found that the C1 whisker map location was stable, but had increased in size, as expected, following chronic whisker trimming sparing only the C1 whisker (**Fig. 5C**). To quantify this effect, we calculated the C1 whisker evoked map area for 6 mice pre- and post-trimming and found an ~82% increase in map area after trimming (**Fig. 5D**, pre-trimming = 0.16 ± 0.03 mm², post-trimming = 0.30 ± 0.03 mm², paired sample, two tailed t-test $p=0.003$). Thus, our IOSI set-up yields highly sensitive, quantitative cortical maps that can be used to both localize cortical signals as well as study fundamental processes such as cortical map plasticity.

Discussion

Here we describe a set of simple adaptations that can be applied to an existing upright microscope to allow high sensitivity IOSI. These adaptations make use of readily

available commercial parts, can be implemented in an afternoon (or less), require no custom machining, and do not require any specialized skills in optics, electronics, circuit design or programming. The entire set-up can be implemented at extremely low cost - ~\$5,000 for an entire set-up or <\$50 if the microscope to be adapted is already equipped with a sufficient camera and objective. In addition, we provide simple MATLAB-based applications for controlling illumination and processing acquired images. Using this set-up we were able to record strong evoked signals from major areas of the mouse somatosensory cortex, including the S1BF, S1FL, S1HL, and V1. These maps show excellent signal-to-noise and are highly reproducible across mice. We were also able to record sensory-evoked signals from smaller cortical areas, consistently generating clear single-whisker evoked cortical maps from several adjacent whiskers that aligned with the expected somatotopy. Finally, we found that our IOSI set-up could be used to quantitatively measure cortical map plasticity, detecting a significant increase in the cortical map area of a spared whisker after chronic whisker trimming.

The IOSI set-up we describe here incorporates methods from previously described IOSI systems with updated, low-cost hardware. The first is hardware for sample illumination. Early IOSI imaging set-ups utilized broadband light sources integrated into the micro- or macroscope housing, collimated and passed through excitation filters (Grinvald et al., 1986; Ratzlaff and Grinvald, 1991). Later iterations incorporated external light sources on flexible light guides to simplify construction (Augustinaite and Kuhn, 2021; Frostig et al., 1995; Nsiangani et al., 2022). More recently, it was recognized that LEDs could provide a stable, low-cost illumination

source for IOSI (Harrison et al., 2009; Salzberg et al., 2005). We choose the LED ring light used here for several reasons: 1) it is commercially available at low cost; 2) it allows for three color illumination (including 525 nm for visualizing vasculature and 625 nm for IOSI); 3) it has integrated drivers and can be controlled with a basic Arduino microcontroller; 4) it is powered by a simple 5V AC/DC power adapter plugged into a standard electrical outlet; and 5) it can be easily mounted using a simple 3D printed mount. Together, these features allow for stable, even illumination of samples that can be connected with just a few wires.

For collection optics, we used an off-the-shelf, commercial 4x plan apochromatic microscope objective. A tandem lens microscope is often used for light collection, given an excellent combination of field-of-view (FOV), working distance, and numerical aperture (Ratzlaff and Grinvald, 1991). However, microscope optics have advanced and now even relatively inexpensive microscope objectives have sufficient numerical apertures (NA of ~ 0.1 - 0.2 , compared to ~ 0.4 for a tandem lens configuration). For cameras, we tested both a CCD and a CMOS scientific microscope camera. Since intrinsic signals are small, ~ 0.01 - 0.1% of total reflected light, having a camera with sufficient sensitivity is essential (Frostig et al., 1995). The cameras we tested here had specifications (and costs) in the mid-range of available scientific cameras in the same class and both were able to achieve qualitatively similar results mapping single-whisker evoked responses. Generally speaking, CCD cameras can achieve higher sensitivity and lower noise compared to CMOS cameras. CCD camera sensors can also perform pixel binning prior to signal readout, resulting in greater sensitivity and signal-to-noise

ratio than can be achieved by CMOS cameras. For cameras with lower sensitivity, such as CMOS cameras, imaging more frames with shorter exposure times (i.e., increasing framerate) can improve signal-to-noise.

Our IOSI set-up does have some limitations. We have not directly compared our system with a traditional tandem-lens microscope. Such purpose-built IOSI rigs are cheaper for labs without an existing microscope available to adapt. The tandem-lens format also offers optical advantages in terms of fewer glasses for reflected light to travel through, potentially larger FOV, and better NA compared to microscope objectives. The LED ring light we used will not fit on larger objectives or tandem lens microscopes. However, the same LEDs are available as larger rings or strings of LEDs that can be shaped into custom forms. As such, the same illumination strategy can be adapted for a range of collection optics, including a tandem-lens configuration. Our illumination control application works well for constant single-wavelength illumination, but is not designed for multi-spectral imaging (Bouchard et al., 2009; White et al., 2011). It should be possible to achieve rapid wavelength switching synchronized to camera acquisition using the hardware we have described, but this would require additional customization. To date, we have used only two cameras in our experiments. We believe a range of modern CCD and CMOS cameras will likely function to achieve IOSI, given the mid-range technical specifications of the tested cameras. When comparing the CCD and CMOS cameras here we did not perform pixel binning and it is likely that the CCD camera would outperform the CMOS camera if this were done. We refer readers to additional resources for choosing a particular camera for their imaging set up, which will

depend on their budget and required sensitivity (Frostig and Chen-Bee, 2009; Harrison et al., 2009).

Regarding field-of-view (FOV), with a 4x objective, we achieved FOVs of $\sim 4.5 \times 3.4$ mm and $\sim 5.7 \times 4.3$ mm with the CCD and CMOS cameras, respectively. These FOV sizes can visualize the most common craniotomy sizes in mice, but may not be sufficient for imaging larger cortical regions or animals. However, larger FOV can be achieved by reducing the magnification on the microscope objective or camera tube lens, utilizing a larger format camera sensor, and/or switching to a tandem lens microscope configuration. Our image processing application allows users to adjust many settings specific to their particular imaging set-up. However, we cannot guarantee functionality for more custom use-cases. In addition, the application generates scaled $\Delta R/R$ images and maps overlaid onto vasculature, but users may require more advanced image processing tools in certain cases (e.g. retinotopic mapping of higher visual cortical areas). Finally, we have not provided detailed instructions here on generating stimuli to evoke cortical signals as we anticipate these will vary significantly from laboratory to laboratory based on individual experimental paradigms.

We envision these adaptations will be best suited to laboratories looking to add IOSI capabilities to an existing upright microscope in the laboratory. The primary advantages include low cost, ease of implementation, and small footprint given that a separate dedicated IOSI rig is not required. However, we anticipate that some of these adaptations or software tools may also be useful for more advanced users wanting to

update components of existing rigs or incorporate these adaptations into custom-built stand-alone IOSI rigs.

References

- Arnett MT, Herman DH, McGee AW (2014) Deficits in tactile learning in a mouse model of fragile X syndrome. *PLoS One* 9:e109116.
- Augustinaite S, Kuhn B (2021) Intrinsic optical signal imaging and targeted injections through a chronic cranial window of a head-fixed mouse. *STAR Protocols* 2:100779.
- Ba AM, Guiou M, Pouratian N, Muthialu A, Rex DE, Cannestra AF, Chen JWY, Toga AW (2002) Multiwavelength optical intrinsic signal imaging of cortical spreading depression. *J Neurophysiol* 88:2726–2735.
- Bakin JS, Kwon MC, Masino SA, Weinberger NM, Frostig RD (1996) Suprathreshold auditory cortex activation visualized by intrinsic signal optical imaging. *Cereb Cortex* 6:120–130.
- Bouchard MB, Chen BR, Burgess SA, Hillman EMC (2009) Ultra-fast multispectral optical imaging of cortical oxygenation, blood flow, and intracellular calcium dynamics. *Opt Express* 17:15670–15678.
- Chen JW, O'Farrell AM, Toga AW (2000) Optical intrinsic signal imaging in a rodent seizure model. *Neurology* 55:312–315.
- Clarkson AN, López-Valdés HE, Overman JJ, Charles AC, Brennan KC, Thomas Carmichael S (2013) Multimodal examination of structural and functional remapping in the mouse photothrombotic stroke model. *J Cereb Blood Flow Metab* 33:716–723.
- Crair MC, Ruthazer ES, Gillespie DC, Stryker MP (1997) Relationship between the ocular dominance and orientation maps in visual cortex of monocularly deprived cats. *Neuron* 19:307–318.
- Daigle TL et al. (2018) A Suite of Transgenic Driver and Reporter Mouse Lines with Enhanced Brain-Cell-Type Targeting and Functionality. *Cell* 174:465-480.e22.
- Dana H, Novak O, Guardado-Montesino M, Franssen JW, Hu A, Borghuis BG, Guo C, Kim DS, Svoboda K (2018) Thy1 transgenic mice expressing the red fluorescent calcium indicator jRGECO1a for neuronal population imaging in vivo. *PLOS ONE* 13:e0205444.
- de Vries SEJ et al. (2020) A large-scale standardized physiological survey reveals functional organization of the mouse visual cortex. *Nat Neurosci* 23:138–151.
- Drew PJ, Feldman DE (2009) Intrinsic signal imaging of deprivation-induced contraction of whisker representations in rat somatosensory cortex. *Cereb Cortex* 19:331–348.
- Dubroff JG, Stevens RT, Hitt J, Maier DL, McCasland JS, Hodge CJ (2005) Use-dependent plasticity in barrel cortex: intrinsic signal imaging reveals functional expansion of spared whisker representation into adjacent deprived columns. *Somatosens Mot Res* 22:25–35.
- Frostig RD, Chen-Bee CH (2009) Visualizing Adult Cortical Plasticity Using Intrinsic Signal Optical Imaging In: *In Vivo Optical Imaging of Brain Function*, *Frontiers in Neuroscience* (Frostig RD ed), Boca Raton (FL): CRC Press/Taylor & Francis.

- Frostig RD, Masino SA, Kwon MC, Chen CH (1995) Using light to probe the brain: Intrinsic signal optical imaging. *Int J Imaging Syst Technol* 6:216–224.
- Gao J, Marosi M, Choi J, Achiro JM, Kim S, Li S, Otis K, Martin KC, Portera-Cailliau C, Tontonoz P (2017) The E3 ubiquitin ligase IDOL regulates synaptic ApoER2 levels and is important for plasticity and learning. *Elife* 6.
- Grinvald A (1985) Real-time optical mapping of neuronal activity: from single growth cones to the intact mammalian brain. *Annu Rev Neurosci* 8:263–305.
- Grinvald A, Lieke E, Frostig RD, Gilbert CD, Wiesel TN (1986) Functional architecture of cortex revealed by optical imaging of intrinsic signals. *Nature* 324:361–364.
- Harrison TC, Sigler A, Murphy TH (2009) Simple and cost-effective hardware and software for functional brain mapping using intrinsic optical signal imaging. *Journal of Neuroscience Methods* 182:211–218.
- Harrison TC, Silasi G, Boyd JD, Murphy TH (2013) Displacement of sensory maps and disorganization of motor cortex after targeted stroke in mice. *Stroke* 44:2300–2306.
- He CX, Cantu DA, Mantri SS, Zeiger WA, Goel A, Portera-Cailliau C (2017) Tactile Defensiveness and Impaired Adaptation of Neuronal Activity in the Fmr1 Knock-Out Mouse Model of Autism. *J Neurosci* 37:6475–6487.
- He Q, Arroyo ED, Smukowski SN, Xu J, Piochon C, Savas JN, Portera-Cailliau C, Contractor A (2019) Critical period inhibition of NKCC1 rectifies synapse plasticity in the somatosensory cortex and restores adult tactile response maps in fragile X mice. *Mol Psychiatry* 24:1732–1747.
- Hippenmeyer S, Vrieseling E, Sigrist M, Portmann T, Laengle C, Ladle DR, Arber S (2005) A developmental switch in the response of DRG neurons to ETS transcription factor signaling. *PLoS Biol* 3:e159.
- Holtmaat A, Bonhoeffer T, Chow DK, Chuckowree J, De Paola V, Hofer SB, Hübener M, Keck T, Knott G, Lee W-CA, Mostany R, Mrcic-Flogel TD, Nedivi E, Portera-Cailliau C, Svoboda K, Trachtenberg JT, Wilbrecht L (2009) Long-term, high-resolution imaging in the mouse neocortex through a chronic cranial window. *Nat Protoc* 4:1128–1144.
- Johnston DG, Denizet M, Mostany R, Portera-Cailliau C (2013) Chronic in vivo imaging shows no evidence of dendritic plasticity or functional remapping in the contralesional cortex after stroke. *Cereb Cortex* 23:751–762.
- Kalatsky VA, Polley DB, Merzenich MM, Schreiner CE, Stryker MP (2005) Fine functional organization of auditory cortex revealed by Fourier optical imaging. *Proc Natl Acad Sci U S A* 102:13325–13330.
- Kalogeraki E, Pielecka-Fortuna J, Löwel S (2017) Environmental enrichment accelerates ocular dominance plasticity in mouse visual cortex whereas transfer to standard cages resulted in a rapid loss of increased plasticity. *PLoS One* 12:e0186999.
- Lau C, Ng L, Thompson C, Pathak S, Kuan L, Jones A, Hawrylycz M (2008) Exploration and visualization of gene expression with neuroanatomy in the adult mouse brain. *BMC Bioinformatics* 9:153.
- Lehmann K, Löwel S (2008) Age-dependent ocular dominance plasticity in adult mice. *PLoS One* 3:e3120.

- Masino SA, Kwon MC, Dory Y, Frostig RD (1993) Characterization of functional organization within rat barrel cortex using intrinsic signal optical imaging through a thinned skull. *Proc Natl Acad Sci U S A* 90:9998–10002.
- Mostany R, Portera-Cailliau C (2008) A craniotomy surgery procedure for chronic brain imaging. *J Vis Exp*.
- Narayan SM, Santori EM, Toga AW (1994) Mapping functional activity in rodent cortex using optical intrinsic signals. *Cereb Cortex* 4:195–204.
- Nsiangani A, Del Rosario J, Yeh AC, Shin D, Wells S, Lev-Ari T, Williams B, Haider B (2022) Optimizing intact skull intrinsic signal imaging for subsequent targeted electrophysiology across mouse visual cortex. *Sci Rep* 12:2063.
- Peirce J, Gray JR, Simpson S, MacAskill M, Höchenberger R, Sogo H, Kastman E, Lindeløv JK (2019) PsychoPy2: Experiments in behavior made easy. *Behav Res* 51:195–203.
- Petersen CCH (2019) Sensorimotor processing in the rodent barrel cortex. *Nat Rev Neurosci* 20:533–546.
- Polley DB, Chen-Bee CH, Frostig RD (1999) Two directions of plasticity in the sensory-deprived adult cortex. *Neuron* 24:623–637.
- Polley DB, Kvasnák E, Frostig RD (2004) Naturalistic experience transforms sensory maps in the adult cortex of caged animals. *Nature* 429:67–71.
- Prakash N, Cohen-Cory S, Frostig RD (1996) RAPID and opposite effects of BDNF and NGF on the functional organization of the adult cortex in vivo. *Nature* 381:702–706.
- Ratzlaff EH, Grinvald A (1991) A tandem-lens epifluorescence microscope: hundred-fold brightness advantage for wide-field imaging. *J Neurosci Methods* 36:127–137.
- Rubin BD, Katz LC (1999) Optical imaging of odorant representations in the mammalian olfactory bulb. *Neuron* 23:499–511.
- Salzberg BM, Kosterin PV, Muschol M, Obaid AL, Rumyantsev SL, Bilenko Yu, Shur MS (2005) An ultra-stable non-coherent light source for optical measurements in neuroscience and cell physiology. *Journal of Neuroscience Methods* 141:165–169.
- Schindelin J, Arganda-Carreras I, Frise E, Kaynig V, Longair M, Pietzsch T, Preibisch S, Rueden C, Saalfeld S, Schmid B, Tinevez J-Y, White DJ, Hartenstein V, Eliceiri K, Tomancak P, Cardona A (2012) Fiji: an open-source platform for biological-image analysis. *Nat Methods* 9:676–682.
- Schuett S, Bonhoeffer T, Hübener M (2002) Mapping retinotopic structure in mouse visual cortex with optical imaging. *J Neurosci* 22:6549–6559.
- Smith SL, Trachtenberg JT (2010) The refinement of ipsilateral eye retinotopic maps is increased by removing the dominant contralateral eye in adult mice. *PLoS One* 5:e9925.
- Trachtenberg JT, Trepel C, Stryker MP (2000) Rapid extragranular plasticity in the absence of thalamocortical plasticity in the developing primary visual cortex. *Science* 287:2029–2032.
- White BR, Bauer AQ, Snyder AZ, Schlaggar BL, Lee J-M, Culver JP (2011) Imaging of functional connectivity in the mouse brain. *PLoS One* 6:e16322.

- Zeiger WA, Marosi M, Saggi S, Noble N, Samad I, Portera-Cailliau C (2021) Barrel cortex plasticity after photothrombotic stroke involves potentiating responses of pre-existing circuits but not functional remapping to new circuits. *Nat Commun* 12:3972.
- Zepeda A, Arias C, Sengpiel F (2004) Optical imaging of intrinsic signals: recent developments in the methodology and its applications. *J Neurosci Methods* 136:1–21.

Figure Legends

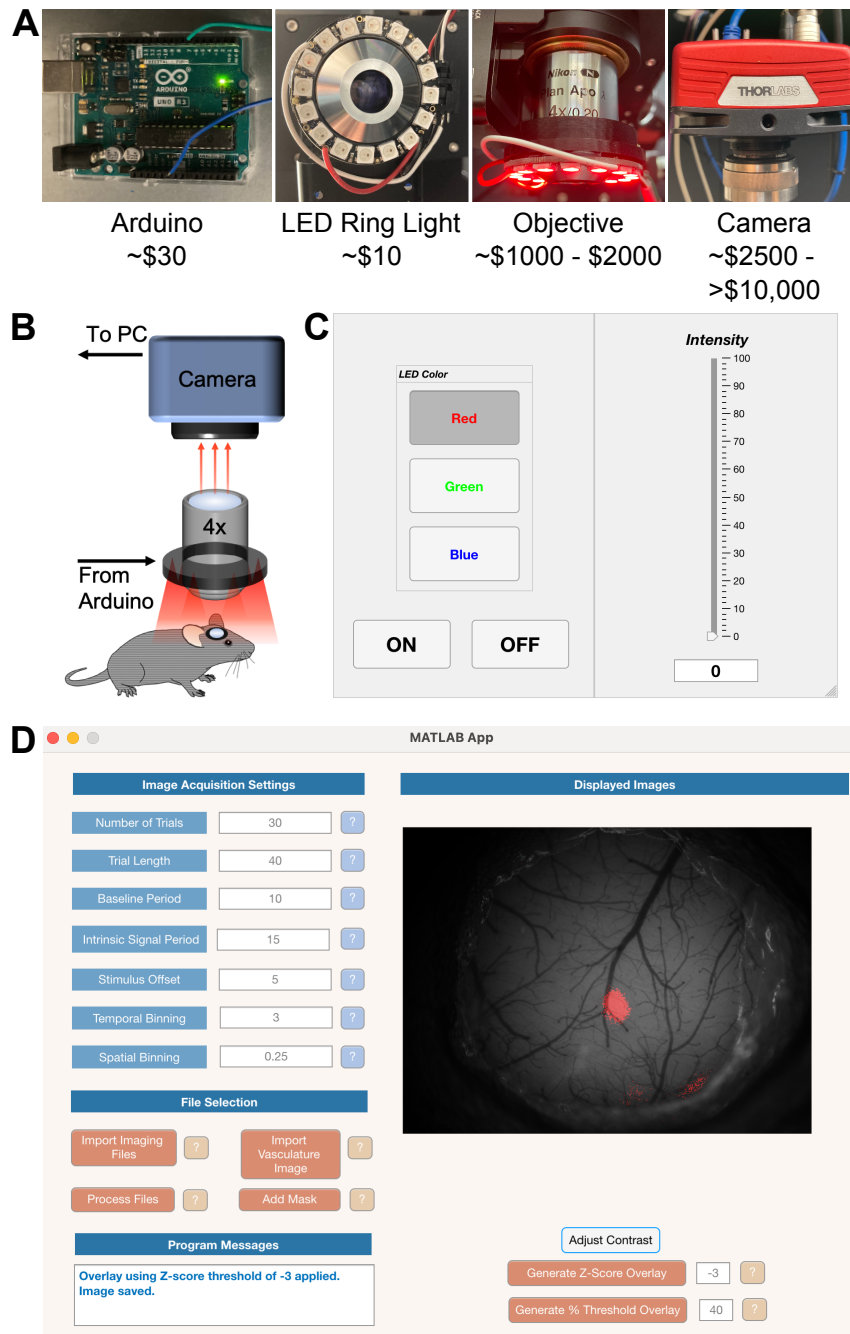


Figure 1. Hardware and Software Adaptations to enable IOSI on an existing upright microscope.

- A.** Hardware necessary to achieve IOSI includes (from left to right) an Arduino microcontroller connection to an LED ring light for illumination, an objective for light collection, and a camera to record reflected light.
- B.** Schematic of the hardware adaptations and basic connections.
- C.** Image of the application for illumination control. Users may set the illumination wavelength and intensity.
- D.** Image of the application for basic image analysis. Users may input settings used for image acquisition and identify acquired images. The application will then process images, calculate $\Delta R/R$ values and display a scaled image in the application window. Thresholding can then be done within the application, using either an absolute percentage of the maximum $\Delta R/R$ value or using Z-scores of $\Delta R/R$ values, and a binarized map can then be overlaid onto an image of the vasculature for localization of signals.

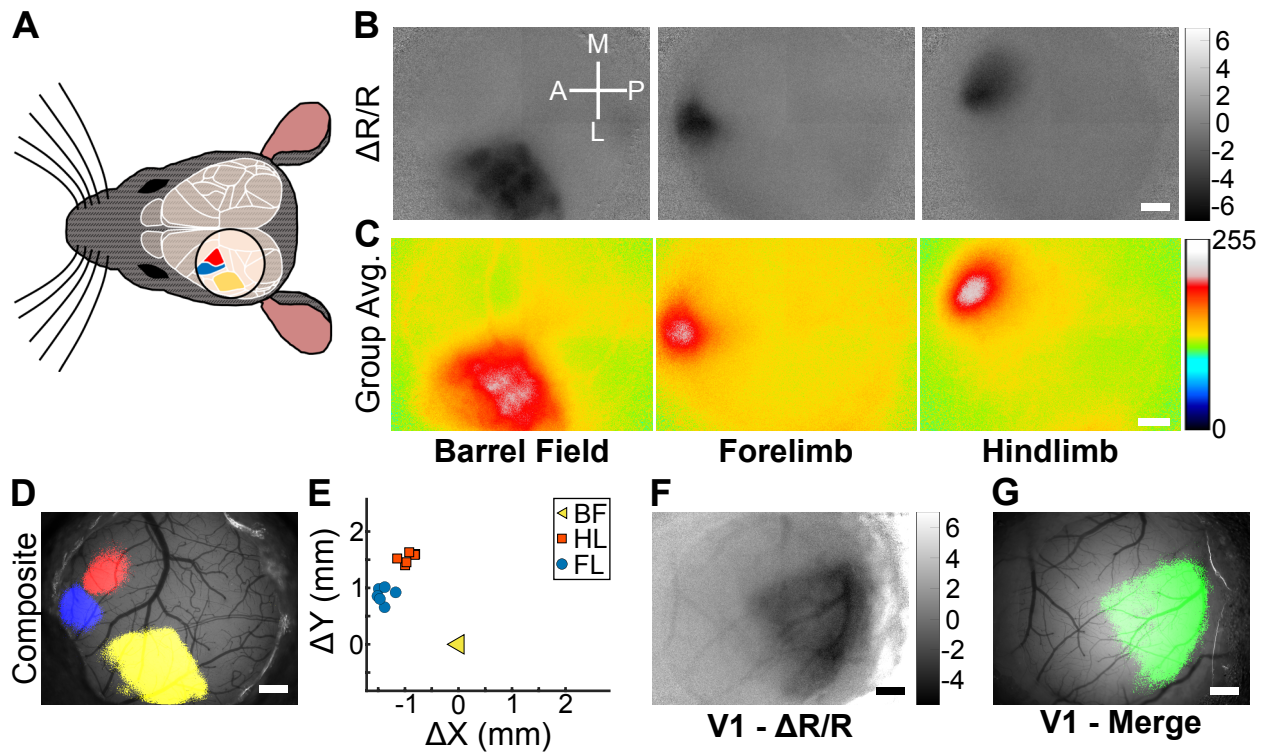


Figure 2. Mapping evoked signals across primary somatosensory and visual cortices.

- A.** Schematic of cranial window placement for mapping evoked signals in the primary somatosensory cortex. Approximate locations of major cortical regions are outlined in white (adapted from the Allen Mouse Brain Atlas Brain Explorer 2), with the S1FL (blue), S1HL (red), and S1BF (yellow) color coded.
- B.** Scaled $\Delta R/R$ images of IOSI from an individual mouse performed during vibrotactile stimulation of the contralateral whiskers, forelimb, or hindlimb. Scaled $\Delta R/R$ values are $\times 10^{-4}$. Scale bar = 0.5 mm.
- C.** Group averaged images from 6 mice of IOSI performed during vibrotactile stimulation of the contralateral whiskers, forelimb, or hindlimb. Values are arbitrary units of 8 bit images from minimum (0) to maximum (255). Scale bar = 0.5 mm.

- D.** Merged sensory-evoked maps from (B) overlaid onto the cortical vasculature. $\Delta R/R$ images were Z-scored and thresholded for values < -3 , binarized, pseudocolored (S1FL [blue], S1HL [red], and S1BF [yellow]), then merged and overlaid. Scale bar = 0.5 mm.
- E.** Displacement of S1FL and S1HL map centers, relative to the S1BF map, from 6 individual mice. Map displacements for S1FL and S1HL were significantly different from one another (one-way MANOVA, $p=1.04 \times 10^{-5}$).
- F.** Scaled $\Delta R/R$ images of IOSI from an individual mouse performed during passive viewing of drifting sinusoidal gratings by the contralateral eye. Scaled $\Delta R/R$ values are $\times 10^{-3}$. Scale bar = 0.5 mm.
- G.** Visual-evoked map from (F) overlaid onto the cortical vasculature. Scale bar = 0.5 mm.

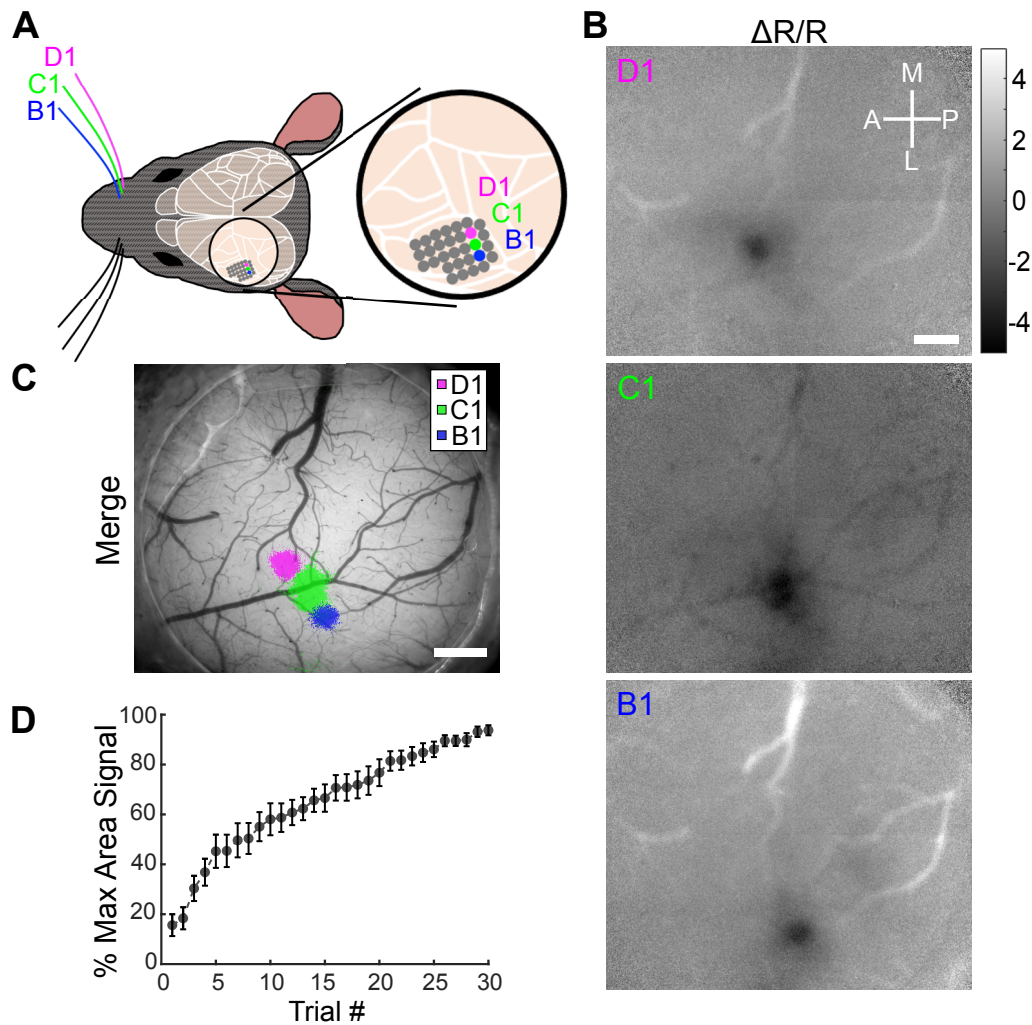


Figure 3. IOSI of single whisker evoked cortical activity in the S1BF

- A.** Schematic of stimulated whiskers (B1, C1, and D1) and somatotopic organization of the corresponding barrels in the S1BF.
- B.** Scaled $\Delta R/R$ images of IOSI from an individual mouse performed during vibrotactile stimulation of the contralateral B1, C1, and D1 whiskers. Scaled $\Delta R/R$ values are $\times 10^{-3}$. Scale bar = 0.5 mm. See Figure 3-1 for scaled $\Delta R/R$ images of IOSI performed using higher framerate acquisition (30 Hz) or acute thinned skull preparation.

- C.** Merged single whisker maps from (B) overlaid onto the cortical vasculature. $\Delta R/R$ images were Z-scored and thresholded for values < -3 , binarized, pseudocolored, then merged and overlaid. Scale bar = 0.5 mm.
- D.** Average map area by IOSI trial, as a percentage of the maximum map area following all 30 trials, of 18 single whisker representations in 6 mice.

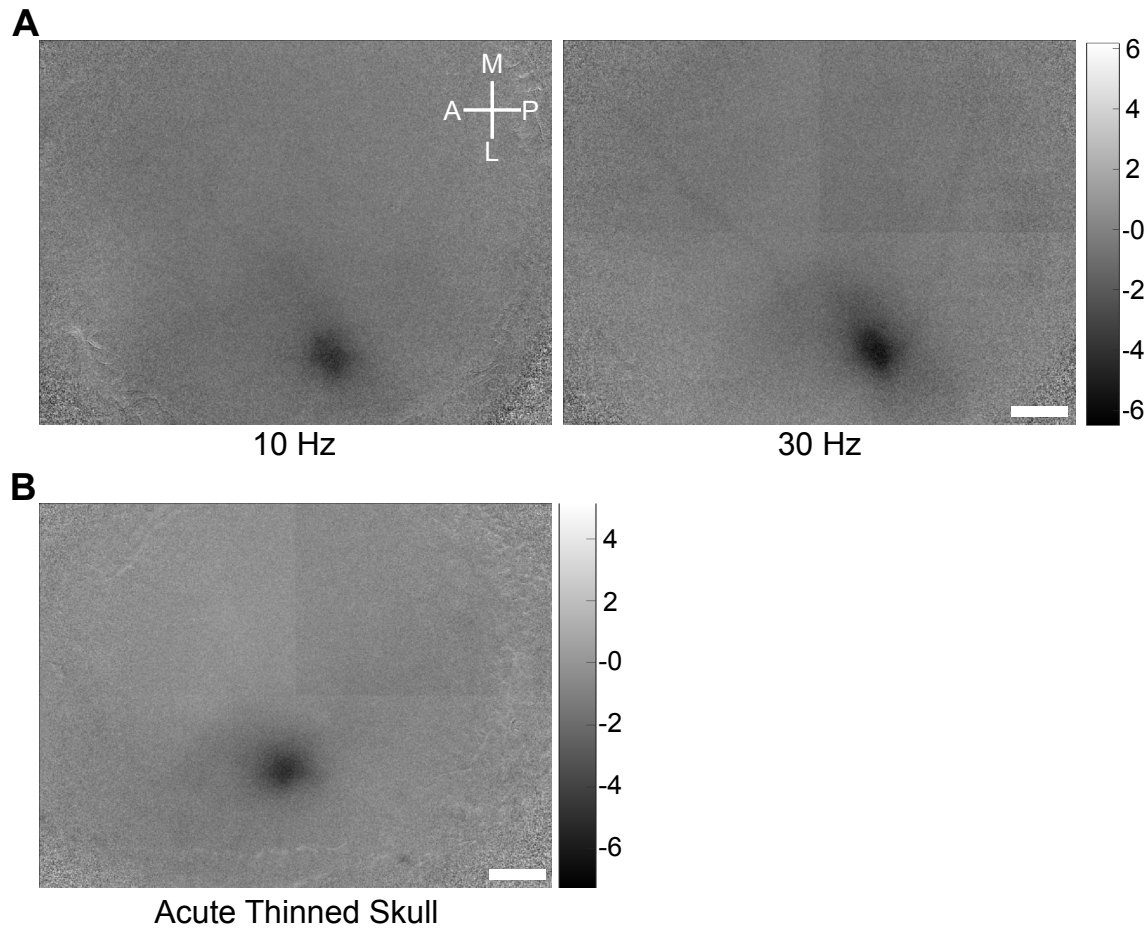


Figure 3-1. IOSI of single whisker evoked cortical activity in the S1BF using higher framerates or an acute thinned skull cranial window

A. Scaled $\Delta R/R$ images of IOSI from an individual mouse performed during vibrotactile stimulation of the contralateral C1 whisker, imaging at 10 Hz (left) or 30 Hz (right).

Scaled $\Delta R/R$ values are $\times 10^{-3}$. Scale bar = 0.5 mm.

B. Scaled $\Delta R/R$ images of IOSI through the acutely thinned skull from an individual mouse performed during vibrotactile stimulation of the contralateral D1 whisker.

Scaled $\Delta R/R$ values are $\times 10^{-3}$. Scale bar = 0.5 mm.

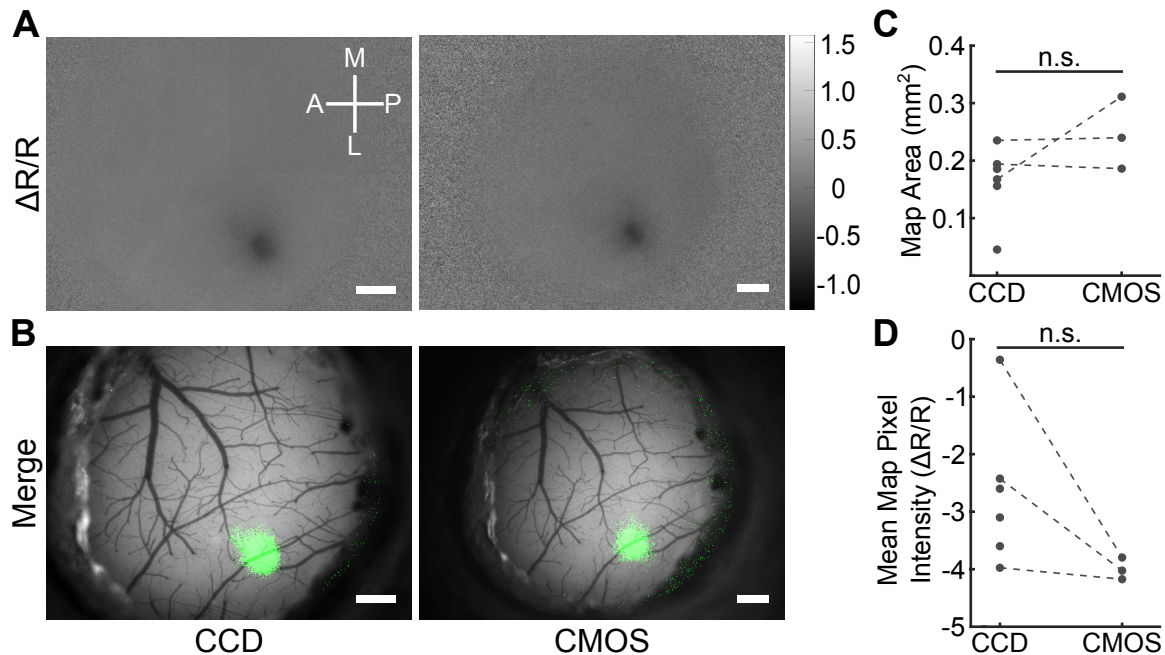


Figure 4. High sensitivity IOSI can be achieved with CCD or CMOS cameras

- A.** Scaled $\Delta R/R$ images of IOSI from an individual mouse performed during vibrotactile stimulation of the contralateral C1 whisker. Scaled $\Delta R/R$ values are $\times 10^{-2}$. Scale bar = 0.5 mm.
- B.** Merged single whisker maps from (A) overlaid onto the cortical vasculature. $\Delta R/R$ images were Z-scored and thresholded for values < -3 , binarized, pseudocolored, then merged and overlaid. Scale bar = 0.5 mm.
- C.** Quantification of C1 single whisker map area from 6 mice imaged with the CCD camera and 3 mice imaged with the CMOS camera. Dotted lines indicate the same mouse imaged with both cameras, with imaging using the CMOS camera performed 6 days after the start of chronic whisker trimming (see **Fig. 5**). Two-tailed t-test, $p=0.13$.
- D.** Quantification of C1 single whisker map mean $\Delta R/R$ pixel intensity from the same mice as in C. $\Delta R/R$ values are $\times 10^{-3}$. Two-tailed t-test, $p=0.11$.

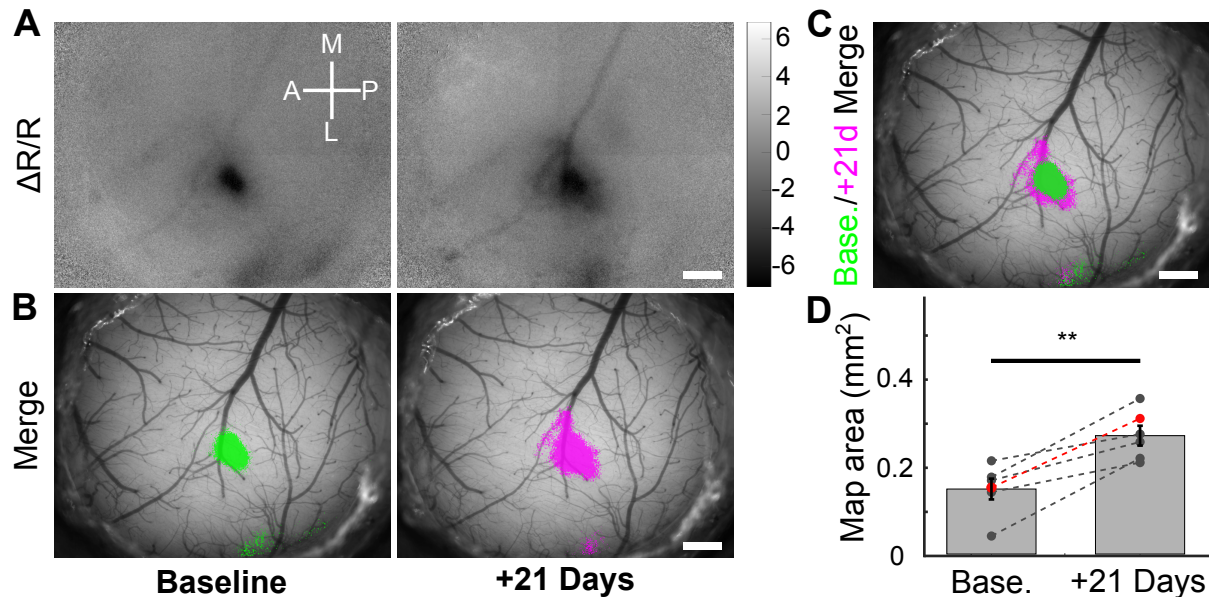


Figure 5. Longitudinal IOSI detects cortical map plasticity following whisker trimming

- A.** Scaled $\Delta R/R$ images of IOSI from an individual mouse performed during vibrotactile stimulation of the contralateral C1 whisker at baseline before (left) and 21 days after whisker trimming sparing only the C1 whisker. Scaled $\Delta R/R$ values are $\times 10^{-3}$. Scale bar = 0.5 mm.
- B.** Merged single whisker maps from (A) overlaid onto the cortical vasculature. $\Delta R/R$ images were Z-scored and thresholded for values < -3 , binarized, pseudocolored, then merged and overlaid. Scale bar = 0.5 mm.
- C.** Merged pre- and post-whisker trimming maps, aligned using vasculature images, showing expansion of the C1 whisker cortical map representation. Scale bar = 0.5 mm.
- D.** Quantification of change in C1 map area after whisker trimming from 6 mice. The dots in red represent the mouse depicted in panels A-C. **, paired sample, two-tailed t-test, $p=0.003$.

Extended Data Legend

ISI Parts List.xlsx – excel spreadsheet listing all materials required to implement the IOSI adaptations described in this manuscript

IOSI_RingLED_IlluminationBuild.docx – word document providing step-by-step instructions for assembling and setting up ring LED illumination

Ring LED Holder-2.stl – Design file to 3D print the mount for the ring LED

NeopixelControl.mlapp – MATLAB application for controlling ring LED illumination

iosgui.mlapp – MATLAB application for processing IOSI data

IOSGUI_ImageAnalysis.m – companion script for processing IOSI data, used by iosgui.mlapp

IOSGUI_Instructions.docx – An instruction manual for using the iosgui application for processing IOSI data